Journal of Molecular Graphics and Modelling 57 (2015) 70–75

Contents lists available at ScienceDirect

Journal of Molecular Graphics and Modelling

journal homepage: www.elsevier.com/locate/JMGM

Removal of trihalomethanes from aqueous solution through armchair carbon nanotubes: A molecular dynamics study

Jafar Azamat [a], Alireza Khataee [a,*], Sang Woo Joo [b,**], Binfeng Yin [b]

[a] Research Laboratory of Advanced Water and Wastewater Treatment Processes, Department of Applied Chemistry, Faculty of Chemistry, University of Tabriz, 51666-14766 Tabriz, Iran
[b] School of Mechanical Engineering, Yeungnam University, Gyeongsan 712-749 South Korea

ARTICLE INFO

Article history:
Accepted 23 January 2015
Available online 3 February 2015

Keywords:
Carbon nanotube
Graphene
Nanostructured membrane
Trihalomethane
Molecular simulations

ABSTRACT

Molecular dynamics simulations were performed to investigate the removal of trihalomethanes (THMs) including CH_3Cl, CH_2Cl_2 and $CHCl_3$ from aqueous solutions by armchair carbon nanotubes (CNTs) under induced pressure. The studied system involved the armchair CNTs embedded between two graphene sheets with an aqueous solution of THMs in the simulation box. An external pressure was applied to the system along the *z*-axis of the simulation box. Six types of armchair CNTs with different diameter were used in this work, included (4,4), (5,5), (6,6), (7,7), (8,8) and (9,9) CNTs. The results of molecular dynamics simulation display that the armchair CNTs behave differently relative to THMs and water molecules. The permeation of THMs and water molecules through the armchair CNTs was dependent on the diameter of CNTs and the applied pressure.

1. Introduction

Drinking water supply is one of the main concerns in countries. The drinking of low quality water causes health hazards in the community. Chlorination of water is one of the disinfection treatment methods [1–3]. This method is one of the most widely used disinfection processes because of low cost, easy utilization and good efficiency [4]. The main objective of chlorination is to kill microorganisms in the water. Water chlorination was started in 1908 in New Jersey and it remains a widely used method of disinfection [5]. Trihalomethanes (THMs) are formed as a by-product predominantly when chlorine is used to disinfect water for drinking. They represent the group of chemicals generally referred to as disinfection by-products (DBPs). These molecules are halogen-substituted single-carbon compounds with the formula CH_nX_m, where *X* can be fluorine, chlorine, bromine or iodine. THMs are formed in the water chlorination process when the chlorine is reacted with humic and fulvic acids [6–9]. THMs have been detected in different aqueous solutions such as: ground and mineral water, tap and swimming pool water, snow, rain, sea and river water [10]. The formation rate of THMs in aqueous solutions increases as a function of the chlorine and humic acid concentration, contact time, pH, dissolved organic carbon, and temperature [11]. THMs are tasteless, odorless, and high volatility but harmful and potentially toxic. They can cause cancer, miscarriage, reproductive problems, and birth defects [12]. Chaidou et al. [13] have shown that chlorination DBPs cause problems in different parts of the human body such as the kidney, liver, and nervous system. In another work, the effect of DBPs on DNA damage at quite low levels in human derived hepatoma line was studied by Zhang et al. [14]. Therefore, removal of chlorination disinfection by-products such as trihalomethanes from water is important.

Up to the present time, many researches have been carried out different methods to reduce THM concentration in water, such as reverse osmosis, and adsorption on activated carbon [15–17]. One of the wastewater treatment methods is membrane technology. Over the past decade, separation processes by membrane have been developed for industrial applications [18,19]. Carbon nanotubes (CNTs) are one of the membranes that can be used in the removal of THMs form aqueous solutions. CNTs with their nano scale diameters, can lead to potential applications in the desalination process [20–26] and diseases treatment [27–30]. The CNTs are characterized by a pair of indexes (*n*,*m*). The indexes *n* and *m* are the number of unit vectors of graphene sheet. Depending on the values of these two indexes, there are three types of CNTs including zigzag ($m = 0$), armchair ($n = m$) and chiral ($n \neq m$).

* Corresponding author. Tel.: +98 4133393165; fax: +98 4133340191.
** Corresponding author. Tel.: +82 53 810 1456.
E-mail addresses: a_khataee@tabrizu.ac.ir, ar_khataee@yahoo.com (A. Khataee), swjoo@yu.ac.kr (S.W. Joo).

http://dx.doi.org/10.1016/j.jmgm.2015.01.008
1093-3263/

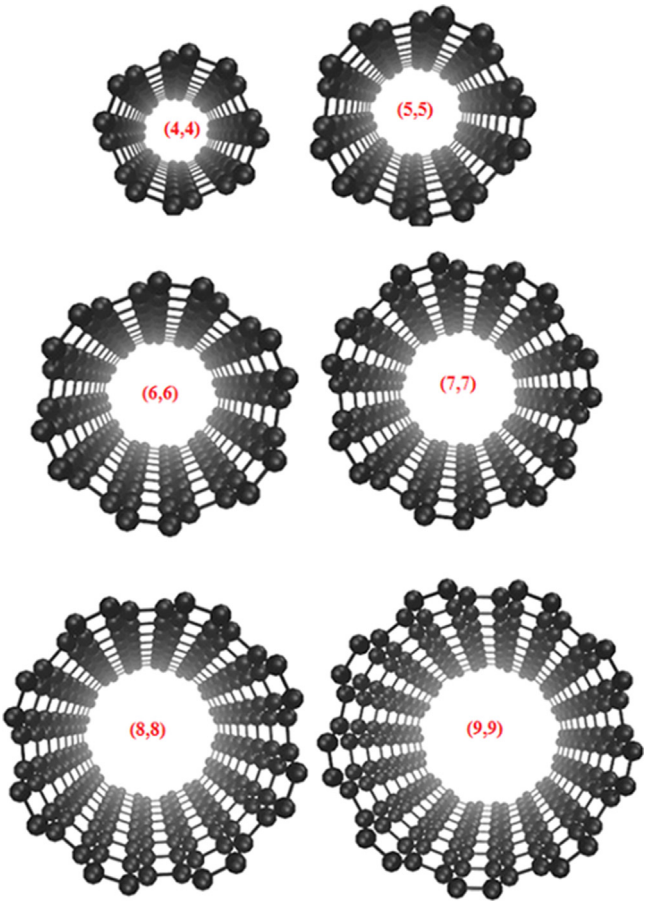

Fig. 1. Schematic layout of the nanotubes studied in this work. CNT (4,4), CNT (5,5), CNT (6,6), CNT (7,7), CNT (8,8), CNT (9,9) with diameters of: 5.49 Å, 6.83 Å, 8.18 Å, 9.53 Å, 10.88 Å and 12.24 Å, respectively.

To the best of our knowledge, no study was reported about the removal of THMs (CH_3Cl, CH_2Cl_2 and $CHCl_3$) from aqueous solution using the armchair CNTs. Therefore, in this work, we studied the removal of THMs from aqueous solutions using armchair CNTs as a membrane under induced pressure using molecular simulation method. Molecular dynamics (MD) simulation is one of the main fields of nanotechnology. Design, production and scale up of various processes can be simulated by this method. In this work, CH_3Cl, CH_2Cl_2, and $CHCl_3$ were used as THMs molecules. The reason for choosing these species was due to their presence in water, after the chlorination process.

2. Simulation methodology

In this research, six types of CNTs with a length of 22 Å were selected, including (4,4), (5,5), (6,6), (7,7), (8,8) and (9,9) CNTs (Fig. 1). A full geometric optimization of the electronic ground state of CNTs and THM molecules was obtained by applying density functional theory (DFT) method. These computations were done at the B3LYP level of theory using 6-311G (2d, 2p) basis sets. All calculations were carried out using GAMESS-US package [31]. The results of DFT for the THMs are given in Table 1. For the CNTs, all carbon atoms are assumed to be electrically neutral [32].

The MD domain was consisted of an armchair CNT embedded between two graphene sheets, with an aqueous solution of THM molecules (Fig. 2). THM molecules used in the simulation were a solution containing equal proportions of all three molecules $CHCl_3$, CH_2Cl_2 and CH_3Cl. The concentration of THM molecules was 0.3 mol/L and the number water molecules in the box were

Table 1
The results of the DFT calculations for THMs.

Type of THMs	CH_3Cl	CH_2Cl_2	$CHCl_3$
Charge of carbon	−0.66	−0.476	−0.351
Charge of hydrogen	+0.248	+0.267	+0.285
Charge of chlorine	−0.083	−0.029	+0.022
Bond length of C—H (Å)	1.089	1.087	1.086
Bond length of C—Cl (Å)	1.804	1.792	1.788

1700 molecules. The simulation box for all runs was ($x \times y \times z$) 30 Å × 30 Å × 80 Å. The periodic boundary conditions with the minimum image convention were used in all three directions to mimic system with an infinitely large area. The short-range interactions for atomic species were described with the Lennard–Jones potential. The water–CNT, water–THMs and THMs–CNT interaction parameters were derived using the Lorentz–Berthelot combining rules. We performed MD simulations with NAMD2.9 [33] similar to previous works [34–37] with a 1 fs time step using a Particle Mesh Ewald (PME) summation for electrostatic interactions calculations [38]. Also, all analysis scripts were composed locally using the VMD1.9.2 [39] and Tcl commands. The empirical CHARMM force field was used for the atoms [40] to describe inter-atomic interactions. Parameters for carbon atoms in the CNTs and graphenes were taken as the parameters for carbon in the CHARMM27 force field [41,42]. To represent water molecules, the intermolecular three point potential (TIP3P) model [43] was employed. Three site models have three interaction points corresponding to the three atoms of the water molecule. Each site has a point charge, and the site corresponding to the oxygen atom also has the Lennard–Jones parameters. Since three site models achieve a high computational efficiency, these are widely used in MD simulations. Most of the models use a rigid geometry matching that of actual water molecules. One of these models is the TIP3P model, which assumes an ideal shape. The potential energy (U_{eff}) for the non-bonded interactions was given by the sum of Lennard–Jones (U_{vdw}) and Coulomb (U_C) potentials through Eq. (1).

$$U_{eff} = U_{vdw} + U_C = 4\sqrt{\varepsilon_i \varepsilon_j}\left[\left(\frac{\sigma_i + \sigma_j}{2r_{ij}}\right)^{12} - \left(\frac{\sigma_i + \sigma_j}{2r_{ij}}\right)^{6}\right] + \frac{q_i . q_j}{4\pi\varepsilon_0 r_{ij}} \quad (1)$$

where r_{ij} is the distance between the fragments i and j; ε_i and σ_i are the Lennard–Jones parameters related to atom i; q_i and q_j are the partial charge assigned to atoms i and j. In this work, the armchair CNT embedded between two graphene sheets was placed in the

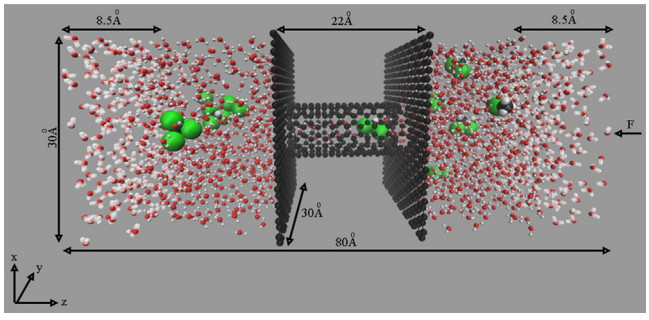

Fig. 2. A snapshot of the simulated system. The simulation box is 30 Å × 30 Å × 80 Å (black color represents carbons atoms; green color represents chlorine atoms; red and white colors represent the oxygen and hydrogen atoms of water molecules, respectively. Two water reservoirs are attached to each side of the box. In the glass region, external forces are applied on water molecules to create a pressure drop across the membrane). (For interpretation of the references to color in this figure legend, the reader is referred to the web version of this article.)

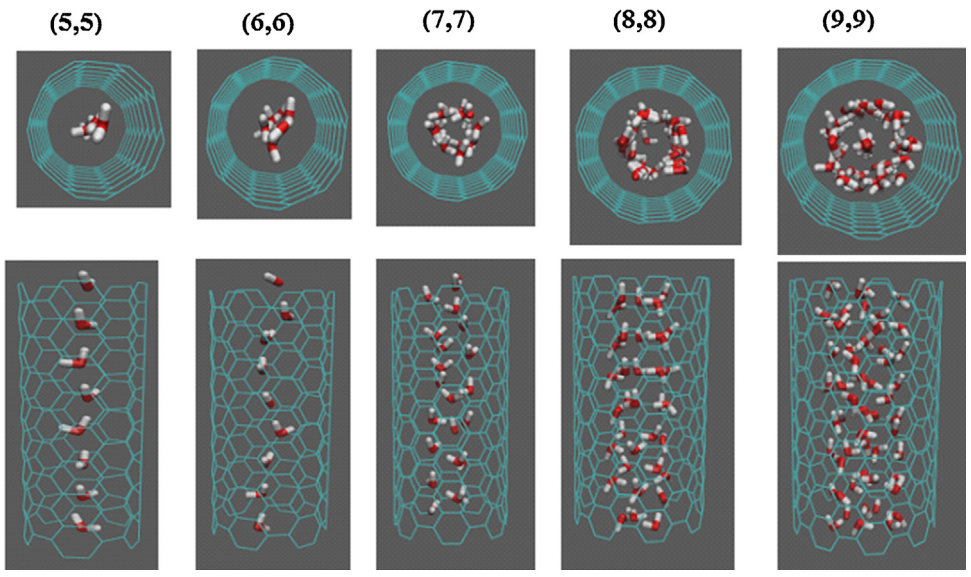

Fig. 3. Arrangement of water molecules inside the studied CNTs.

center of the box and both of them were fixed during the simulation time. It was shown that the flexibility of CNTs only affected the kinetics of transport into a CNT when the pore entrance was about the same size as the molecule [44]. Van der Waals interactions were truncated smoothly by means of a 12 Å spherical cutoff in conjunction with a switching function. The system was subjected to a zero-temperature energy minimization for 0.5 ns and, equilibrated for 1 ns at 298 K. Then 5 ns MD simulations were performed. The Langevin dynamics method [45] was used to keep the temperature at 298 K.

The external constant forces were applied in the z direction of system to the oxygen atom of water molecules in a selected area of the system (within a distance of 8.5 Å of the left or right boundary of the system). These forces cause a pressure gradient through the CNTs. For this purpose, a method developed by Zhu et al. [46,47] was used in our system. This method was used for pressure-driven flow in many literatures [48–51]. The applied constant force was given by Eq. (2):

$$F = \frac{\Delta P \cdot A}{n} \tag{2}$$

where F is a force applied to the selected region of system, ΔP is the chosen pressure, A is the area of the system, and n is the number of water molecules in the selected area (see Fig. 2). Pressure range was in the range of 10–200 MPa and it was applied to approximately 560 water molecules.

3. Results and discussion

In this research, six types of armchair CNTs were used to investigate the removal of THMs using MD simulations method. The MD results showed THMs and water molecules could not pass through the (4,4) CNT. But, in the (5,5) CNT, water molecules could pass through this CNT and THMs remained on one side of box. In contrast, in the large CNTs, in addition to water molecules, THM molecules with different ratios could pass through them.

Each water molecule can form four hydrogen bonds with neighboring water molecules. Probably, this structure helps, at least within a short range, to give water its unique properties. The interaction of THMs with water can lead to breaking the structure of water and ensuring the arrangement of water molecules. Fig. 3 displays the arrangement of water molecules inside the studied CNTs. As can be seen, water molecules lied in different arrangement inside the CNTs. The radial distribution function (RDF) water–CNT showed the structures of water molecules inside the CNTs (Fig. 4). RDF is a measure representing the probability of finding a particle at a distance of r away from a given reference particle. Fig. 4 shows

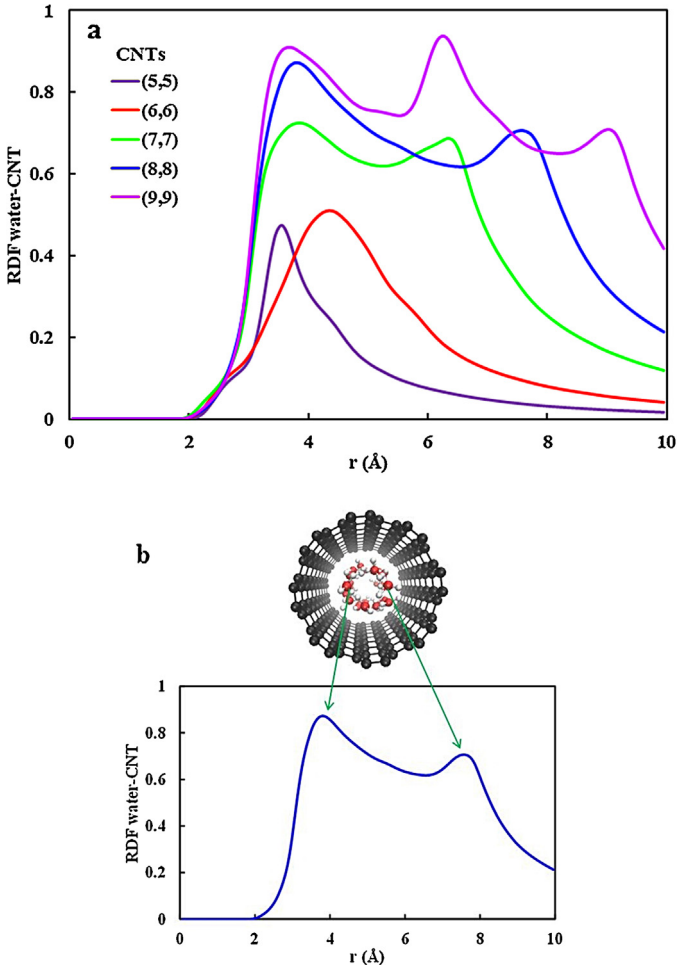

Fig. 4. (a) Water–CNT radial distribution functions in the simulation box. (b) Schematic layout of the water–(8,8) CNT RDF. *Note*: scales are not considered in this figure.

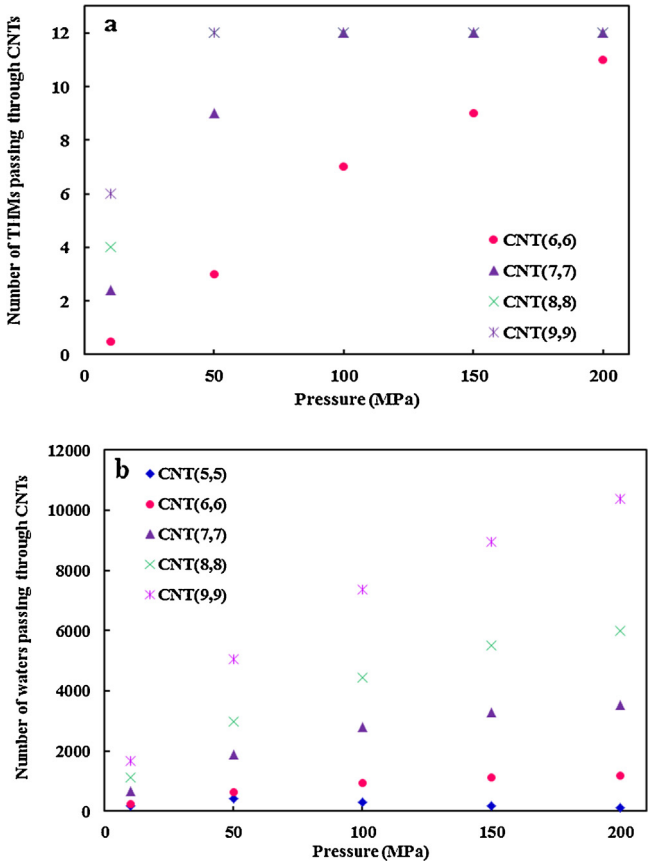

Fig. 5. The number of (a) THMs and (b) water molecules passing through the CNTs. (In the small CNTs, only water molecules can pass through the CNT.)

the RDF between water molecules and CNTs (as reference particle). The positions and number of peak varied in each nanotube because of different arrangements of water molecules inside the CNTs. The single file structure of water molecules inside the (5,5) and (6,6) CNTs was changed to the spiral mode in the (7,7) and (8,8) CNTs. This restructuring of the water molecules was due to the increasing diameter of CNTs. The single file structure of water molecules inside the (5,5) and (6,6) CNTs was shown with a peak in the RDF. In the case of (7,7) and (8,8) CNTs, RDF had two peaks that are in conformity with the spiral structure of water (Fig. 4b). In the case of (9,9) CNT, in addition to the spiral mode, the single file structure was also observed. The (9,9) CNT RDF showed three peaks. A peak was for the single file structure of water molecules and two peaks were related to the spiral structure of water molecules.

As noted, the number of THMs and water molecules passing through the CNTs was different. As can be seen in Fig. 5, the number of THMs and water molecules passing through CNTs increased with increasing the applied pressures. Both THMs and water molecules were able to pass through the (6,6), (7,7), (8,8) and (9,9) CNTs. By increasing the diameter of the CNT, the flow rate of water was increased too. It should be reminded that the THMs could not be transferred through small CNTs ((4,4), (5,5)).

The only exception can be seen in Fig. 5b. In the case of (5,5) CNT, we expected that with increasing the pressure, the water flow rate was increased, but this trend was changed in the pressure of 50 MPa. From this point onwards, with increasing the pressure, the flow rate of water was reduced. The creation of blocked space in front of (5,5) CNT by THMs can be its reason. THM molecules remained in the span of CNT and prevented the passage of water molecules from it.

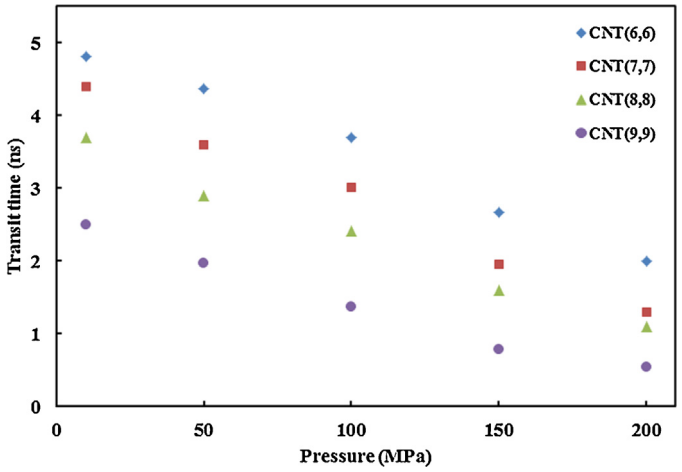

Fig. 6. Transit time of THMs across different CNTs under various applied pressures.

As observed before, THMs crossed from different large CNTs at the high pressures. But, the important parameter was the time required to remove all THMs from CNTs (transit time). This time was decreased with increasing the applied pressure as shown in Fig. 6. Also, the transit time had downtrend with increasing the diameter of the CNTs.

In this work, the retention time of THMs, i.e., the time of passing one THM through the CNT, was investigated. The MD results showed that the retention time of THMs did not depend on the applied pressures and its value was constant.

Fig. 7 shows the number of water molecules inside the CNTs based on the applied pressures. As can be seen, the number of water molecules inside a CNT with increasing the pressure is not changed and being always constant. But, it increases by increasing the diameter of CNTs. Consequently, the number of hydrogen bonds between the inner water molecules inside CNTs is also raised by increasing the diameter of CNTs (Fig. 8).

Fig. 9 shows the density profile of THMs in three types of the CNTs under applied pressures. They are calculated from the final frame of the MD simulations. These density profiles were calculated in the pressure of 200 MPa for the (5,5) and (9,9) CNTs and 10 MPa for the (8,8) CNT. As previously noted, THMs did not pass through small CNTs and so remain on one side of the box (red line). In the case of (9,9) CNT, all THMs were removed from contaminated water (purple line). It must be noted that in the (8,8) CNT under low

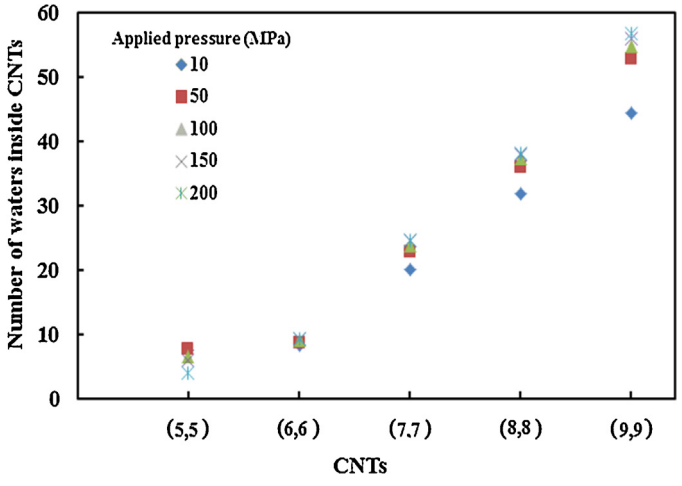

Fig. 7. Number of water inside CNTs under various applied pressures.

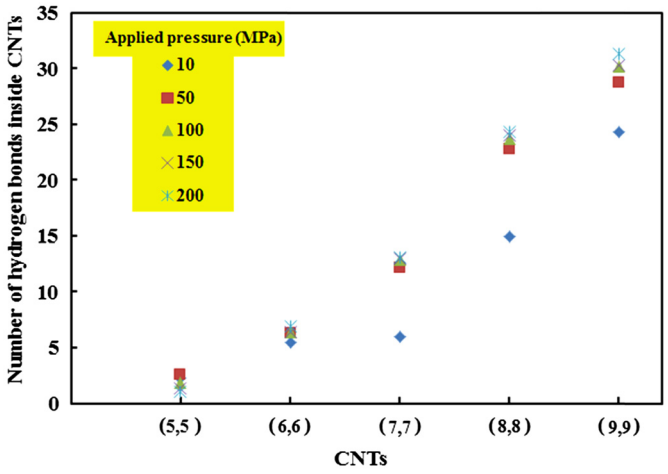

Fig. 8. Number of hydrogen bonds inside the CNTs under various applied pressures.

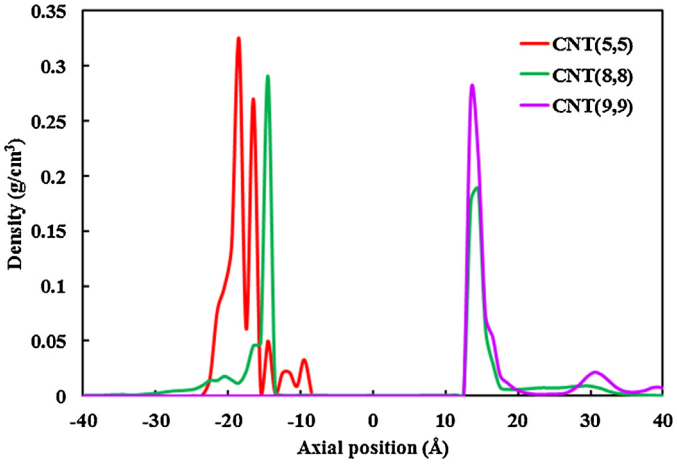

Fig. 9. Density profile of THMs in three type of the CNTs in the simulation time in z direction of system (red line: none of THMs are passed through the (5,5) CNT under 200 MPa pressure; green line: some of THMs are separated from contaminated water by the (8,8) CNT under 10 MPa pressure; purple line: all THMs are separated from contaminated water by the (9,9) CNT under 200 MPa pressure). (For interpretation of the references to color in this figure legend, the reader is referred to the web version of this article.)

pressure (10 MPa), some THMs were removed from the contaminated water (green line). The non-permeation of THM for the (5,5) CNT was occurred under other applied pressures. But in the case of (8,8) CNT, in high applied pressures, a full permeation of THMs were occurred with different transit time as shown in Fig. 6. This time for a specified pressure (such as 200 MPa) for the (9,9) CNT was less than the that of (8,8) CNT.

4. Conclusion

The removal of THMs (CH_3Cl, CH_2Cl_2 and $CHCl_3$) by various armchair CNTs embedded between two graphene sheets was studied by MD simulations method. It was shown that the removal of THMs from aqueous solution through CNTs occurred in the presence of applied pressures. The armchair CNTs with different diameters could effectively remove THMs from water. THMs and water molecules were passed through the large CNTs with different transit times. In contrast, just water molecules were passed through (5,5) CNT, and THMs molecules were filtered.

Acknowledgments

This work is funded by the Iranian National Science Foundation (INSF) through the grant #92030491. The authors sincerely thank to the INSF and the University of Tabriz for providing all of the support.

References

[1] R. Sadiq, M.J. Rodriguez, Disinfection by-products (DBPs) in drinking water and predictive models for their occurrence: a review, Sci. Total Environ. 321 (2004) 21–46.
[2] T. Karanfil, Disinfection By-Products in Drinking Water: Occurrence, Formation, Health Effects, and Control, Oxford University Press, Washington, 2008.
[3] H. Baribeau, Formation and Decay of Disinfection By-Products in the Distribution System, IWA Publishing, Denver, 2006.
[4] R.L. Jolley, Water chlorination: environmental impact and health effects, in: Proceedings of the Conference on Water Chlorination: Environmental Impact and Health Effects, Ann Arbor Science Publishers, Ann Arbor, 1980.
[5] T. Ivahnenko, J.S. Zogorski, Sources and occurrence of chloroform and other trihalomethanes in drinking-water supply wells in the United States, U.S. Geological Survey Scientific Investigations Report, Virginia, 2006.
[6] X. Yang, C. Shang, C. Huang, DBP formation in breakpoint chlorination of wastewater, Water Res. 39 (2005) 4755–4767.
[7] P. Westerhoff, P. Chao, H. Mash, Reactivity of natural organic matter with aqueous chlorine and bromine, Water Res. 38 (2004) 1502–1513.
[8] S.C. Gad, Trihalomethanes, in: Encyclopedia of Toxicology, Elsevier, New York, 2005, pp. 389–391.
[9] K. Gopal, S.S. Tripathy, J.L. Bersillon, S.P. Dubey, Chlorination byproducts, their toxicodynamics and removal from drinking water, J. Hazard. Mater. 140 (2007) 1–6.
[10] G.L. Culp, R.C. Gumerman, N. Heim, Trihalomethane Reduction in Drinking Water: Technologies, Costs, Effectiveness, Monitoring, Compliance, Noyes Publications, Park Ridge, NJ, 1984.
[11] A.D. Nikolaou, S.K. Golfinopoulos, G.B. Arhonditsis, V. Kolovoyiannis, T.D. Lekkas, Modeling the formation of chlorination by-products in river waters with different quality, Chemosphere 55 (2004) 409–420.
[12] S. Wang, C. Deng, F. Lin, Cancer risk assessment from trihalomethanes in drinking water, Sci. Total Environ. 387 (2007) 86–95.
[13] C.I. Chaidou, V.I. Georgakilas, C. Stalikas, M. Saraçi, E.S. Lahaniatis, Formation of chloroform by aqueous chlorination of organic compounds, Chemosphere 39 (1999) 587–594.
[14] L. Zhang, L. Xu, Q. Zeng, H. Zhang, H. Xie, L. Liu, W.Q. Lu, Comparison of DNA damage in human-derived hepatoma line (HepG2) exposed to the fifteen drinking water disinfection byproducts using the single cell gel electrophoresis assay, Mutat. Res. Genet. Toxicol. 741 (2012) 89–94.
[15] C. Lu, Y.-L. Chung, K.-F. Chang, Adsorption of trihalomethanes from water with carbon nanotubes, Water Res. 39 (2005) 1183–1189.
[16] D. Ma, B. Gao, S. Sun, Y. Wang, Q. Yue, Q. Li, Effects of dissolved organic matter size fractions on trihalomethanes formation in MBR effluents during chlorine disinfection, Bioresour. Technol. 136 (2013) 535–541.
[17] A. Li, C. Tai, Z. Zhao, Y. Wang, Q. Zhang, G. Jiang, J. Hu, Debromination of decabrominated diphenyl ether by resin-bound iron nanoparticles, Environ. Sci. Technol. 41 (2007) 6841–6846.
[18] J. Azamat, J. Sardroodi, The permeation of potassium and chloride ions through nanotubes: a molecular simulation study, Monatshefte Chem. 145 (2014) 881–890.
[19] J.J. Sardroodi, J. Azamat, A. Rastkar, N.R. Yousefnia, The preferential permeation of ions across carbon and boron nitride nanotubes, Chem. Phys. 403 (2012) 105–112.
[20] R. Das, M.E. Ali, S.B.A. Hamid, S. Ramakrishna, Z.Z. Chowdhury, Carbon nanotube membranes for water purification: a bright future in water desalination, Desalination 336 (2014) 97–109.
[21] M.A. Tofighy, Y. Shirazi, T. Mohammadi, A. Pak, Salty water desalination using carbon nanotubes membrane, Chem. Eng. J. 168 (2011) 1064–1072.
[22] P.S. Goh, A.F. Ismail, B.C. Ng, Carbon nanotubes for desalination: performance evaluation and current hurdles, Desalination 308 (2013) 2–14.
[23] C.H. Ahn, Y. Baek, C. Lee, S.O. Kim, S. Kim, S. Lee, S.-H. Kim, S.S. Bae, J. Park, J. Yoon, Carbon nanotube-based membranes: fabrication and application to desalination, J. Ind. Eng. Chem. 18 (2012) 1551–1559.
[24] S. Kar, R.C. Bindal, P.K. Tewari, Carbon nanotube membranes for desalination and water purification: challenges and opportunities, Nano Today 7 (2012) 385–389.
[25] A. Khataee, S. Aber, M. Zarei, M. Sheydaei, Environmental Applications of Activated Carbon and Carbon Nanotubes, NOVA Science Publisher, Inc., USA, 2011.
[26] F. Taghavi, S. Javadian, S.M. Hashemianzadeh, Molecular dynamics simulation of single-walled silicon carbide nanotubes immersed in water, J. Mol. Graph. Model. 44 (2013) 33–43.
[27] U. Arsawang, O. Saengsawang, T. Rungrotmongkol, P. Sornmee, K. Wittayanarakul, T. Remsungnen, S. Hannongbua, How do carbon nanotubes serve as carriers for gemcitabine transport in a drug delivery system? J. Mol. Graph. Model. 29 (2011) 591–596.

[28] B.R. Meher, Y. Wang, Binding of single walled carbon nanotube to WT and mutant HIV-1 proteases: analysis of flap dynamics and binding mechanism, J. Mol. Graph. Model. 38 (2012) 430–445.
[29] Y. Cheng, D. Li, B. Ji, X. Shi, H. Gao, Structure-based design of carbon nanotubes as HIV-1 protease inhibitors: atomistic and coarse-grained simulations, J. Mol. Graph. Model. 29 (2010) 171–177.
[30] M. Leonor Contreras, D. Ávila, J. Alvarez, R. Rozas, Computational algorithms for fast-building 3D carbon nanotube models with defects, J. Mol. Graph. Model. 38 (2012) 389–395.
[31] M.W. Schmidt, K.K. Baldridge, J.A. Boatz, S.T. Elbert, M.S. Gordon, J.H. Jensen, S. Koseki, N. Matsunaga, K.A. Nguyen, S. Su, T.L. Windus, M. Dupuis, J.A. Montgomery, General atomic and molecular electronic structure system, J. Comput. Chem. 14 (1993) 1347–1363.
[32] Y. Shim, Y. Jung, H.J. Kim, Carbon nanotubes in benzene: internal and external solvation, Phys. Chem. Chem. Phys. 13 (2011) 3969–3978.
[33] L. Kalé, R. Skeel, M. Bhandarkar, R. Brunner, A. Gursoy, N. Krawetz, J. Phillips, A. Shinozaki, K. Varadarajan, K. Schulten, NAMD2: greater scalability for parallel molecular dynamics, J. Comput. Phys. 151 (1999) 283–312.
[34] J. Azamat, A. Khataee, S. Joo, Separation of a heavy metal from water through a membrane containing boron nitride nanotubes: molecular dynamics simulations, J. Mol. Model. 20 (2014) 1–9.
[35] J. Azamat, A. Khataee, S.W. Joo, Functionalized graphene as a nanostructured membrane for removal of copper and mercury from aqueous solution: a molecular dynamics simulation study, J. Mol. Graph. Model. 53 (2014) 112–117.
[36] J. Azamat, J.J. Sardroodi, Ion and water transport through (7,7) and (8,8) carbon and boron nitride nanotubes of different electric fields: a molecular dynamics simulation study, J. Comput. Theor. Nanosci. 11 (2014) 2611–2617.
[37] J. Azamat, J.J. Sardroodi, A. Rastkar, Water desalination through armchair carbon nanotubes: a molecular dynamics study, RSC Adv. 4 (2014) 63712–63718.
[38] G. Ciccotti, D. Frenkel, I.R. McDonald, Simulation of Liquids and Solids, North Holland, New York, 1987.
[39] W. Humphrey, A. Dalke, K. Schulten, VMD: visual molecular dynamics, J. Mol. Graph. 14 (1996) 33–38.
[40] A.D. MacKerell, D. Bashford, M. Bellott, R.L. Dunbrack, J.D. Evanseck, M.J. Field, S. Fischer, J. Gao, H. Guo, S. Ha, D. Joseph-McCarthy, L. Kuchnir, K. Kuczera, F.T.K. Lau, C. Mattos, S. Michnick, T. Ngo, D.T. Nguyen, B. Prodhom, W.E. Reiher, B. Roux, M. Schlenkrich, J.C. Smith, R. Stote, J. Straub, M. Watanabe, J. Wiórkiewicz-Kuczera, D. Yin, M. Karplus, All-atom empirical potential for molecular modeling and dynamics studies of proteins, J. Phys. Chem. B 102 (1998) 3586–3616.
[41] S.E. Feller, A.D. MacKerell, An improved empirical potential energy function for molecular simulations of phospholipids, J. Phys. Chem. B 104 (2000) 7510–7515.
[42] J.B. Klauda, B.R. Brooks, A.D. MacKerell, R.M. Venable, R.W. Pastor, An ab initio study on the torsional surface of alkanes and its effect on molecular simulations of alkanes and a DPPC bilayer, J. Phys. Chem. B 109 (2005) 5300–5311.
[43] D.J. Price, C.L. Brooks, A modified TIP3P water potential for simulation with Ewald summation, J. Chem. Phys. 121 (2004) 10096–10103.
[44] B.J. Bucior, L. Chen, J. Liu, J.K. Johnson, Porous carbon nanotube membranes for separation of H_2/CH_4 and CO_2/CH_4 mixtures, J. Phys. Chem. C 116 (2012) 25904–25910.
[45] X. Wu, B.R. Brooks, Self-guided Langevin dynamics simulation method, Chem. Phys. Lett. 381 (2003) 512–518.
[46] F. Zhu, E. Tajkhorshid, K. Schulten, Pressure-induced water transport in membrane channels studied by molecular dynamics, Biophys. J. 83 (2002) 154–160.
[47] F. Zhu, E. Tajkhorshid, K. Schulten, Theory and simulation of water permeation in aquaporin-1, Biophys. J. 86 (2004) 50–57.
[48] B. Corry, Designing carbon nanotube membranes for efficient water desalination, J. Phys. Chem. B 112 (2008) 1427–1434.
[49] X. Gong, J. Li, H. Lu, R. Wan, J. Li, J. Hu, H. Fang, A charge-driven molecular water pump, Nat. Nanotechnol. 2 (2007) 709–712.
[50] J. Li, X. Gong, H. Lu, D. Li, H. Fang, R. Zhou, Electrostatic gating of a nanometer water channel, PNAS 104 (2007) 3687–3692.
[51] J. Goldsmith, C.C. Martens, Pressure-induced water flow through model nanopores, Phys. Chem. Chem. Phys. 11 (2009) 528–533.